

Scott I. K. Semple
Fiona J. Gilbert
Thomas W. Redpath
Roger T. Staff
Trevor S. Ahearn
Andrew E. Welch
Steven D. Heys
Andrew W. Hutcheon
Elizabeth H. Smyth
Shailesh Chaturvedi

The relationship between vascular and metabolic characteristics of primary breast tumours

Received: 21 April 2004
Revised: 15 July 2004
Accepted: 22 July 2004
Published online: 14 August 2004
© Springer-Verlag 2004

S. I. K. Semple (✉) · F. J. Gilbert
Department of Radiology,
University of Aberdeen,
Lilian Sutton Building, Aberdeen,
AB252ZD, Scotland, UK
e-mail: s.semple@abdn.ac.uk
Tel.: +44-1224-559725
Fax: +44-1224-559718

T. W. Redpath · R. T. Staff · T. S. Ahearn
A. E. Welch
Departments of Bio-Medical Physics
and Bio-Engineering,
University of Aberdeen,
Aberdeen, AB252ZD, Scotland, UK

S. D. Heys
Department of Surgery,
University of Aberdeen,
Aberdeen, AB252ZD, Scotland, UK

A. W. Hutcheon
Department of Clinical Oncology,
Aberdeen Royal Infirmary,
Grampian University Hospitals NHS Trust,
Foresterhill, Aberdeen, AB252ZD,
Scotland, UK

E. H. Smyth · S. Chaturvedi
Departments of Surgery and Pathology,
Grampian University Hospitals NHS Trust,
Foresterhill, Aberdeen, AB252ZD,
Scotland, UK

Abstract The objective of this study was to investigate the relationship between vascular and metabolic characteristics of breast tumours in vivo, using contrast-enhanced dynamic MRI and 2- ^{18}F fluoro-2-deoxy-D-glucose (FDG) PET imaging. Twenty patients with large or locally advanced primary breast cancers were imaged prior to therapy. MRI data were acquired using a dynamic gradient echo sequence and analysed using two pharmacokinetic models. Static PET data were acquired in 2D mode. A significant association ($P < 0.05$) was observed between the calculated exchange rate constants of both pharmacokinetic models and calculated PET FDG dose uptake ratios (DUR). Statistical analysis showed that the exchange rate constants can explain between 27 and 44% of the variance observed in the PET FDG uptake ratios. A relationship was demonstrated between the vascular and metabolic characteristics of primary breast tumours showing that any assessment of tumour metabolic activity using PET may be controlled at least in part by delivery of uptake agent due to the vascular

characteristics of the tumour. MRI and PET provide methods of assessing breast tumour vascularity and metabolism in vivo using the exchange rate constants of dynamic MRI, and DUR of PET, respectively, these measures being related but not equivalent.

Keywords Breast cancer · Dynamic MRI · FDG PET · Kinetic modelling

Introduction

In order for cancer drug therapies to be developed successfully, a fundamental understanding of tumour physiology is essential. Although based on different physiological mechanisms, similarities in vascular contrast enhancement and metabolic tracer uptake patterns in large

breast tumours have recently been observed [1]. If it is assumed that contrast uptake is an analogue for drug delivery, then lack of contrast agent uptake due to lack of delivery infers a lack of drug delivery.

During dynamic contrast-enhanced magnetic resonance imaging (DCE-MRI), analysis of the contrast agent enhancement curve obtained after injection, re-

flecting the vascular characteristics of the tumour, has been shown to be an important factor in the initial diagnosis of breast cancer as well as the detection of response to therapy [2–7]. A number of multi-compartmental models have been successfully applied to describe MR contrast uptake in breast tumours [8, 9].

It has previously been demonstrated that positron emission tomography (PET) metabolic activity imaging using the glucose analogue 2- ^{18}F fluoro-2-deoxy-D-glucose (^{18}F -FDG) may be used as a sensitive indicator of metabolic activity in breast cancers [10, 11]. Malignant cells have an elevated glycolytic rate that has been shown to fall significantly in response to effective chemotherapy [12–14].

Intuitively, one would expect MRI contrast agent enhancement and PET ^{18}F -FDG uptake to be linked through the delivery of nutrients and oxygen [15]. For example, ^{18}F -FDG uptake would not be expected to occur in a region that has no vascular supply. However, Brix et al. [15] previously observed no correlation between MRI pharmacokinetic parameters (derived using a two compartment model) and PET FDG uptake assessed by standard uptake value (SUV) calculations when 14 patients were studied prior to treatment.

We have investigated the relationship between the metabolic and vascular characteristics of primary breast tumours using ^{18}F -FDG PET and DCE-MRI, respectively, addressing some of the issues raised in previous work, in particular, homogeneity of population, range of models and range of assessment techniques. The MRI results were analysed with the application of the two and three compartment models as used by Brix et al. [15] and Hayes et al. [6] in order to assess any influence due to choice of model. We also investigated the effect of deriving single parameter values for an average tumour enhancement curve, as adopted by Brix et al. [15], compared with the hot-spot approach adopted by Hayes et al. [6].

Methods

Patients and study protocol

Patients presenting to the Breast Unit at Aberdeen Royal Infirmary were diagnosed as having breast cancer using standard triple assessment [clinical examination, imaging (mammography and ultrasound) and fine-needle aspiration cytology]. Histological confirmation of breast cancer was obtained by core biopsy. Patients with large T2 or T3 cancers (>3 cm by clinical examination) or locally advanced (T4 with any N status, N2 status with any T size) breast cancers were invited to take part in this study. Contraindications for inclusion were patient claustrophobia or the presence of metal implant for MRI and diabetes for PET. No potential patients exhibited any of these contraindications. Seven patients who were approached were unable to participate for either technical or personal reasons.

Patient characteristics are listed in Table 1. The population comprised 20 females (median age 51.5 years, age range 35–63

Table 1 Patient details. Abbreviations: IDC invasive ductal carcinoma, ILC invasive lobular carcinoma. Tumour volume assessed using MRI semi-automated analysis (expressed in cm^3). Differential uptake ratio (DUR) assessed using PET

Patient no.	Age	Tumour type/grade	Days between MRI and PET	Tumour volume	DUR
1	63	IDC/3	1	62.5	0.0772
2	63	IDC/1	0	0.864	0.0249
3	37	IDC/3	0	70.1	0.107
4	54	IDC/2	2	8.79	0.0586
5	35	IDC/3	0	3.62	0.0276
6	61	IDC/3	0	20.5	0.153
7	55	IDC/3	0	21.5	0.0887
8	53	IDC/1	0	8.08	0.0264
9	44	ILC/2	0	3.19	0.0292
10	54	IDC/2	0	14.8	0.0628
11	49	IDC/3	0	4.75	0.0701
12	58	IDC/3	1	34.3	0.0963
13	37	IDC/1	0	4.35	0.0281
14	44	IDC/3	0	6.90	0.0783
15	55	IDC/2	4	5.79	0.0257
16	50	IDC/1	0	1.61	0.0188
17	39	IDC/1	5	8.08	0.0691
18	39	IDC/3	0	17.7	0.0434
19	63	IDC/3	0	22.4	0.0685
20	44	IDC/3	0	9.20	0.0686

years). Patients received a DCE-MRI scan and ^{18}F -FDG PET scan prior to commencement of cancer therapy. DCE-MRI and PET were ideally performed on the same day as shown in Table 1. Fully informed written consent was obtained from each patient prior to entry as approved by the local ethical committee.

MRI protocol

MR scans were obtained using a 1.5-T NVi/CVi scanner (GE, Waukesha, WI) and four-channel phased array receive only open breast array coil (MRI Devices, Waukesha, WI). Following three-plane localisation, a 3D fast spoiled gradient echo (FSPGR) was obtained in the coronal plane, covering both breasts. The total acquisition time (TA) for this scan was 1 min 43 s. This 3D scan was used to locate the lesion and position subsequent 2D scans. Next, a 2D FSPGR (nine slices) was acquired centred through the tumour ensuring complete coverage of the lesion. Acquisition parameters were as follows: TE/TR=4.2/8.4 ms, $\alpha=6^\circ$, field of view (FOV) = $340 \times 340 \text{ mm}^2$, slice thickness = 5.0 mm, matrix size = 256×256 with 50% phase FOV acquired with phase encoding in the AP direction (TA=10 s). This sequence was then repeated with flip angles of 10° and 35° in order to calculate pre-contrast T_1 , required for the modelling process, as outlined below. The 35° sequence was then repeated over 40 time points (temporal resolution: 10 s) with an intravenous injection of 0.2 mmol/kg gadopentetate dimeglumine (Magnevist, Schering Health Care Ltd, Burgess Hill, UK) administered on the fifth temporal frame using a SPECTRIS MR compatible pump injector (MEDRAD, Pittsburgh, PA) at a rate of 3 ml/s, immediately followed by 20 ml saline flush administered at the same rate. The pump injector ensured standardised bolus injection of contrast agent for all examinations, and the 2D multi-slice sequence that was employed had good temporal resolution over a relatively long acquisition period (TA=6 min 41 s) giving multiple data points and therefore allowing more accurate curve fitting. The 3D FSPGR was then repeated with acquisition parameters as before and then repeated with fat-saturation applied (with TR extended to accommodate the fat-saturation such that TA=3 min 34 s).

PET protocol

Patients were imaged using a CTI ECAT EXACT-31 scanner (Siemens, Erlangen, Germany), which has an axial FOV of 10.8 cm producing 31 tomographic planes simultaneously with a spatial resolution of 6–8 mm in the axial and both transaxial directions. For standardise blood glucose levels, patients fasted for at least 4 h before PET imaging. Patients were imaged prone on a purpose-built couch analogous to the MRI breast coil such that the patients were imaged in the same position for MRI and PET. The PET protocol consisted of a 10-min transmission/attenuation scan acquired 60 min after a 185 MBq injection of ^{18}F -FDG (synthesised on site). This was followed by a 10-min static emission scan. A deconvolution technique was used to correct for scatter that has been shown to reduce scatter into surrounding regions of the reconstructed image to less than 1% [16].

Patient blood glucose was ascertained via a blood sample obtained immediately after examination. Emission data were acquired in 2D mode and reconstructed using a filtered back-projection algorithm with Hanning windowing.

Image analysis-MRI

MR images were transferred to a PC workstation and analysed using purpose-written software in the programming language IDL (Research Systems, Inc., Boulder, CO). An experienced radiologist defined a region of interest (ROI) for each slice within the 2D acquisition enclosing the periphery of the tumour volume and surrounding tissue using a combination of pre-contrast and post-contrast images (see Fig. 1). The ROI was deliberately selected to be larger than the tumour boundaries. Tumour boundaries were determined within the ROI using a semi-automated programme, which defines the tumour volume according to a pre-defined enhancement criterion, which we selected to be an enhancement of 50% by the tenth dynamic frame. An erosion and dilation operation automatically discounts (potentially extraneous) lone voxels (in an attempt to discount blood vessels), and a region-growing algorithm was used to include any regions of low or non-enhancement in tumour centres (a rim enhancement pattern was noted in several cases). Tumour volumes calculated using this method are presented in Table 1.

The proton density weighted ($\alpha=6^\circ, 10^\circ$) and static T_1 weighted (35°) images were used to calculate a T_1 map of both breasts using a Levenberg-Marquardt best-fit algorithm for each voxel. It has previously been shown that small inaccuracies in T_1 estimation can cause up to 45% variations in estimation of pharmacokinetic parameters and that a best-fit approach taking into account slice profile is necessary to calculate an accurate pre-contrast T_1 value [17]. The method employed in this study took into account any possible effects of a non-rectangular slice profile on the effective flip angle by numerically integrating across 100 points through a simulated slice profile during calculation of T_1 . The RF profile was confirmed to be a single lobe truncated sinc pulse with Hanning windowing applied.

Pharmacokinetic analysis was performed according to the Tofts three compartment model [18] and the Brix two compartment model [19, 20]. The assumptions of both models are outlined in the 1999 paper by Tofts et al. [21]. The Tofts model describes contrast enhancement using two parameters, the volume transfer constant of contrast agent K^{trans} (min^{-1}) and the extravascular extracellular (EES) fractional volume v_E (%). The Brix model describes contrast enhancement using three parameters, an amplitude A reflecting the degree of MR signal enhancement, an exchange rate constant k_{21} (min^{-1}) characterising the initial increase of the signal-time curves and an elimination rate k_{el} (min^{-1}) for assessment of the late post-contrast (“wash-out”) phase. A Levenberg-Marquardt algorithm was used to perform a least-squares fit of the observed signal curves to both models using a range of starting

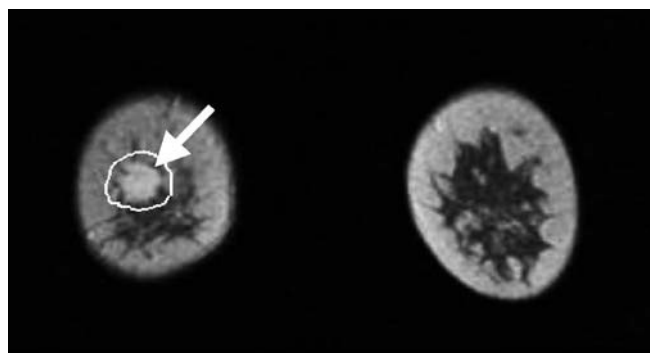


Fig. 1 Typical post-contrast coronal MRI image showing tumour (as indicated by *white arrow*) with manually selected ROI (shown in *white outline*)

values for each model, with automatic selection of the best fit as assessed by the resultant χ^2 values. This approach has previously been shown to improve the accuracy of model fitting to data [22].

Two approaches were adopted for the analysis of pharmacokinetic parameters. Firstly, an analysis similar to that performed by Brix et al. [15] was adopted whereby a mean enhancement curve was calculated for the tumour (with tumour borders being defined using the semi-automated programme outlined above). Both models were then fitted to this mean enhancement curve to generate single pharmacokinetic values for each tumour, hereby referred to as the “mean values”. Secondly, a hot-spot analysis similar to that adopted by Hayes et al. [6] was implemented. For this analysis, pharmacokinetic parameters were fitted for both models on a voxel-by-voxel basis within the tumour and the region of highest rate constant (K^{trans} for Tofts and k_{21} for Brix) was selected. Hayes et al. [6] adopted user-selection of each hot-spot, allowing variability of size. In an attempt to remove operator bias we adopted automatic selection of a $3 \times 3 \times 3$ voxel volume that contained the highest mean transfer constant value over a 27-voxel volume. This selection is performed using a $3 \times 3 \times 3$ matrix that automatically searches in three dimensions throughout the tumour for the $3 \times 3 \times 3$ region of highest transfer constant. We chose this 27-voxel approach as a three dimensional adaptation of a two dimensional analysis by Tsuboi et al., who use a fixed 25-voxel size region to analyse changes in contrast-enhancement curves in patients undergoing preoperative chemotherapy [4]. These 27-voxel volume values are hereby referred to as the “hot-spot values”. A typical single voxel enhancement curve, along with the resultant fits for each model, is displayed in Fig. 2. A typical parametric map of the voxel-by-voxel fit of the Tofts model, along with automatically selected “hot-spot” is displayed in Fig. 3.

Image analysis-PET

Dose uptake ratios (DUR) were calculated for the PET images as given by:

$$DUR = \text{concentration in image} \times \frac{\text{body surface area}}{\text{injected activity}} \quad (1)$$

A typical PET static emission scan is presented in Fig. 4. DUR values were generated for each voxel, then a ROI was selected around the tumour area on the slice that bisected the centre of the tumour. The ROI was manually selected by a radiologist to encompass the periphery of the tumour and surrounding tissue. This ROI was applied to the central tumour slice and two slices on either side of the central slice from which a mean DUR was generated that included contributions from all voxels within the five-

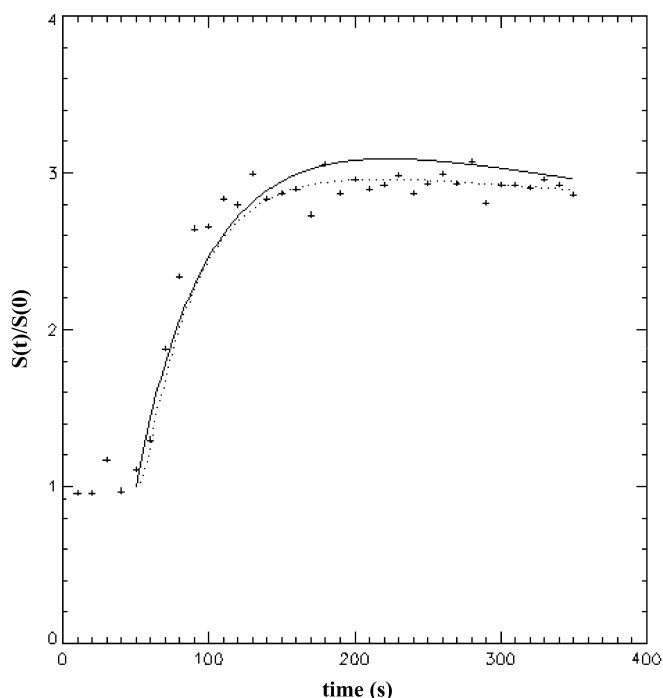


Fig. 2 Relative signal enhancement curve for a single voxel (actual data points shown as *symbols*), with fitted pharmacokinetic curves using Tofts model (*solid line*) and Brix model (*hashed line*). Fitted parameters for this example are: Tofts model $K^{\text{trans}}=0.744 \text{ min}^{-1}$, $v_E=71.6\%$, with χ^2 goodness of fit value = 0.633; Brix model $A=2.08$, $k_{21}=1.61 \text{ min}^{-1}$, $k_{e1}=0.0220 \text{ min}^{-1}$, with χ^2 value = 0.413

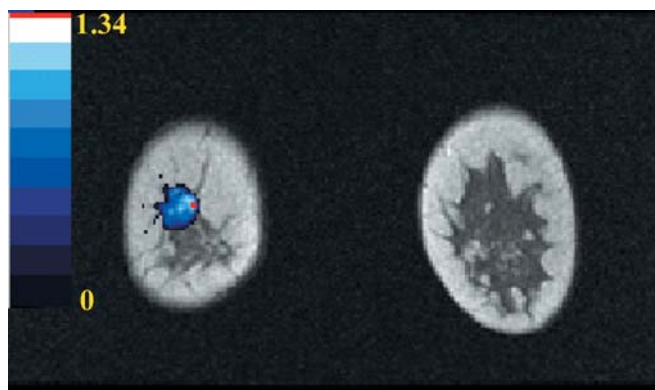


Fig. 3 Typical post-contrast coronal MRI image with K^{trans} voxel map overlay (shown in *blue* with scale indicated, units in min^{-1}), with automatically selected “hot-spot” of highest K^{trans} values (shown in *red*)

slice ROI which exhibited a DUR greater than 80% of the maximum DUR for the ROI. This methodology was selected as an adaptation of a previously published PET analysis protocol [14].

Statistical analysis

All statistical analysis was performed using SPSS for Windows version 11.0 (SPSS, Inc., Chicago, IL). A Kolmogorov-Smirnov

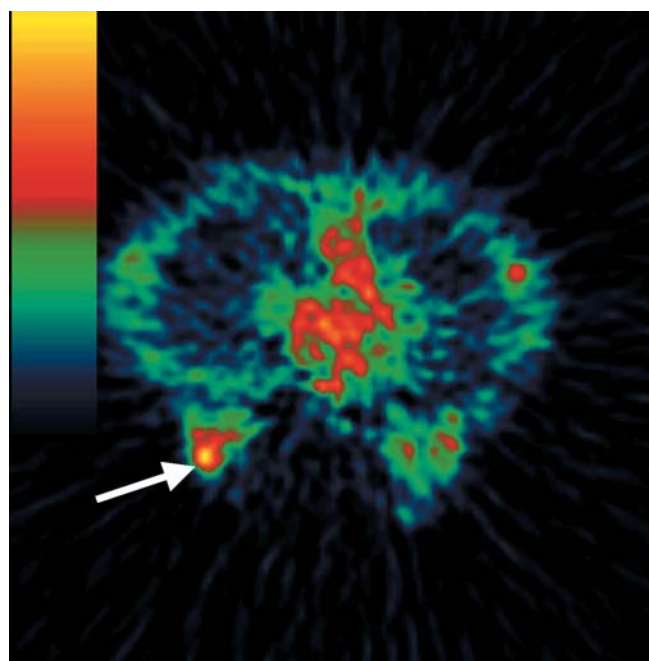


Fig. 4 Typical transaxial PET emission image (shown with *colour scale at left*) with tumour indicated by *white arrow*

(K-S) test was used to assess whether a given parameter distribution differed significantly from a non-normal distribution and could therefore be analysed parametrically. A general linear model was applied to assess the level of dependence of DUR on the MR parameters when a normal distribution could be assumed. In accordance with the statistical analysis performed by Brix et al. [15], a non-parametric Spearman’s rank correlation coefficient P_S was also calculated to assess any correlation between two samples when a normal distribution was not assumed. All statistical tests were performed to a level of $P < 0.05$.

Results

PET DUR values are presented in Table 1. MRI calculated pharmacokinetic values for both models using the mean and hot-spot analysis methods outlined above are presented in Tables 2, 3, respectively.

As with all statistical analysis, we first considered whether we could consider these calculated parameters to be distributed normally. Results of the K-S distribution test showed that both the mean curve and hot-spot values for all MR parameters generated using both models, as well as DUR values, did not differ significantly ($P > 0.11$) from a normal distribution. We therefore used general linear modelling to test the association of each MRI parameter with DUR. The partial η^2 values generated using this approach are estimates of the effect size. These values may also be expressed as the proportion of DUR variance that can be explained by each MR parameter and are equivalent to the square of a correlation type measure (r). These results are shown in Table 4

Table 2 Pharmacokinetic parameters calculated from mean tumour contrast uptake curve. Tofts model K^{trans} and v_E . Brix model A , k_{21} , and k_{el}

Patient no.	Mean K^{trans} (min ⁻¹)	Mean v_E (%)	Mean A	Mean k_{21} (min ⁻¹)	Mean k_{el} (min ⁻¹)
1	0.392	63.0	1.35	0.965	0.0144
2	0.133	47.2	0.387	0.73	-0.0695
3	0.473	27.6	0.589	8.79	-0.0415
4	0.315	27.9	0.508	1.98	-0.00119
5	0.330	39.3	0.389	1.47	-0.00659
6	0.697	42.3	0.672	3.30	0.0000110
7	0.474	29.0	0.568	3.30	-0.00283
8	0.689	54.7	1.31	3.04	-0.0228
9	0.593	62.6	1.42	1.33	0.0371
10	0.765	38.9	1.05	3.44	0.0223
11	0.535	40.7	0.802	4.17	-0.0380
12	0.331	39.4	0.673	2.07	-0.0464
13	0.437	46.6	0.816	2.25	-0.0376
14	0.451	44.6	1.09	1.52	0.0232
15	0.343	40.4	0.681	1.76	-0.0267
16	0.402	51.1	0.575	1.32	0.00141
17	0.486	37.5	0.768	1.89	0.0316
18	0.203	24.7	0.241	2.50	-0.0671
19	0.300	36.0	0.723	1.83	-0.0364
20	0.720	45.1	0.793	3.38	-0.00223

Table 3 Pharmacokinetic parameters calculated from hot-spot analysis. Hot-spot Tofts model K^{trans} and v_E calculated from 27-voxel volume exhibiting highest mean K^{trans} value within tumour ROI. Hot-spot Brix model A , k_{21} , and k_{el} calculated from 27-voxel volume exhibiting highest mean k_{21} value within tumour ROI

Patient no.	Hot-spot K^{trans} (min ⁻¹)	Hot-spot v_E (%)	Hot-spot A	Hot-spot k_{21} (min ⁻¹)	Hot-spot k_{el} (min ⁻¹)
1	1.30	98.0	1.33	1.54	-1.08×10 ⁻⁶
2	0.154	63.5	0.541	2.62	-3.32×10 ⁻⁶
3	2.27	43.3	4.69	10.9	-2.92×10 ⁻⁶
4	1.65	47.6	0.468	12.3	-9.29×10 ⁻⁸
5	0.633	50.7	0.231	4.44	-1.41×10 ⁻⁶
6	1.74	58.5	0.189	28.6	-2.15×10 ⁻⁶
7	1.32	50.6	1.06	4.80	1.36×10 ⁻⁶
8	1.47	65.2	1.75	4.44	5.32×10 ⁻⁷
9	0.763	69.7	1.77	1.50	1.91×10 ⁻⁶
10	2.26	81.6	0.962	7.16	-8.81×10 ⁻⁷
11	0.897	48.5	0.510	25.7	-2.31×10 ⁻⁶
12	1.06	46.9	1.13	3.87	1.16×10 ⁻⁶
13	0.851	64.0	1.24	2.82	-1.27×10 ⁻⁶
14	0.752	53.3	1.95	1.96	3.15×10 ⁻⁶
15	0.580	48.6	1.07	2.34	-9.257×10 ⁻⁷
16	0.653	66.3	0.970	1.43	1.31×10 ⁻⁷
17	1.07	65.8	0.117	2.34	1.37×10 ⁻⁶
18	0.695	55.9	0.114	15.4	-1.84×10 ⁻⁶
19	0.933	71.1	0.384	3.70	-3.52×10 ⁻⁷
20	2.67	80.8	0.640	5.88	2.27×10 ⁻⁶

Table 4 Results of general linear model analysis of MR parameters association with DUR (assumes normal distribution of variables). *Denotes significant association to $P<0.05$ level

	A	k_{21}	k_{el}	K^{trans}	v_E
Mean curve	$\eta^2=0.016$ $p=0.62$	$\eta^2=0.27$ $p=0.028^*$	$\eta^2=0.074$ $p=0.27$	$\eta^2=0.19$ $p=0.064$	$\eta^2=0.18$ $p=0.069$
Hot-spot	$\eta^2=0.13$ $p=0.14$	$\eta^2=0.44$ $p=0.0030^*$	$\eta^2=0.14$ $p=0.12$	$\eta^2=0.33$ $p=0.010^*$	$\eta^2=0.084$ $p=0.23$

with k_{21} exhibiting a significant association ($P<0.05$) with DUR for both the mean curve ($\eta^2=0.27$) and hot-spot analysis ($\eta^2=0.44$) such that the k_{21} values can explain between 27 and 44% of the variance found in the DUR values. K^{trans} exhibited a significant associa-

tion ($P<0.05$) with DUR for the hot-spot analysis ($\eta^2=0.33$), but not the mean curve approach. Scatter plots of mean k_{21} versus DUR, hot-spot k_{21} versus DUR and hot-spot K^{trans} versus DUR are shown in Fig. 5a–c, respectively.

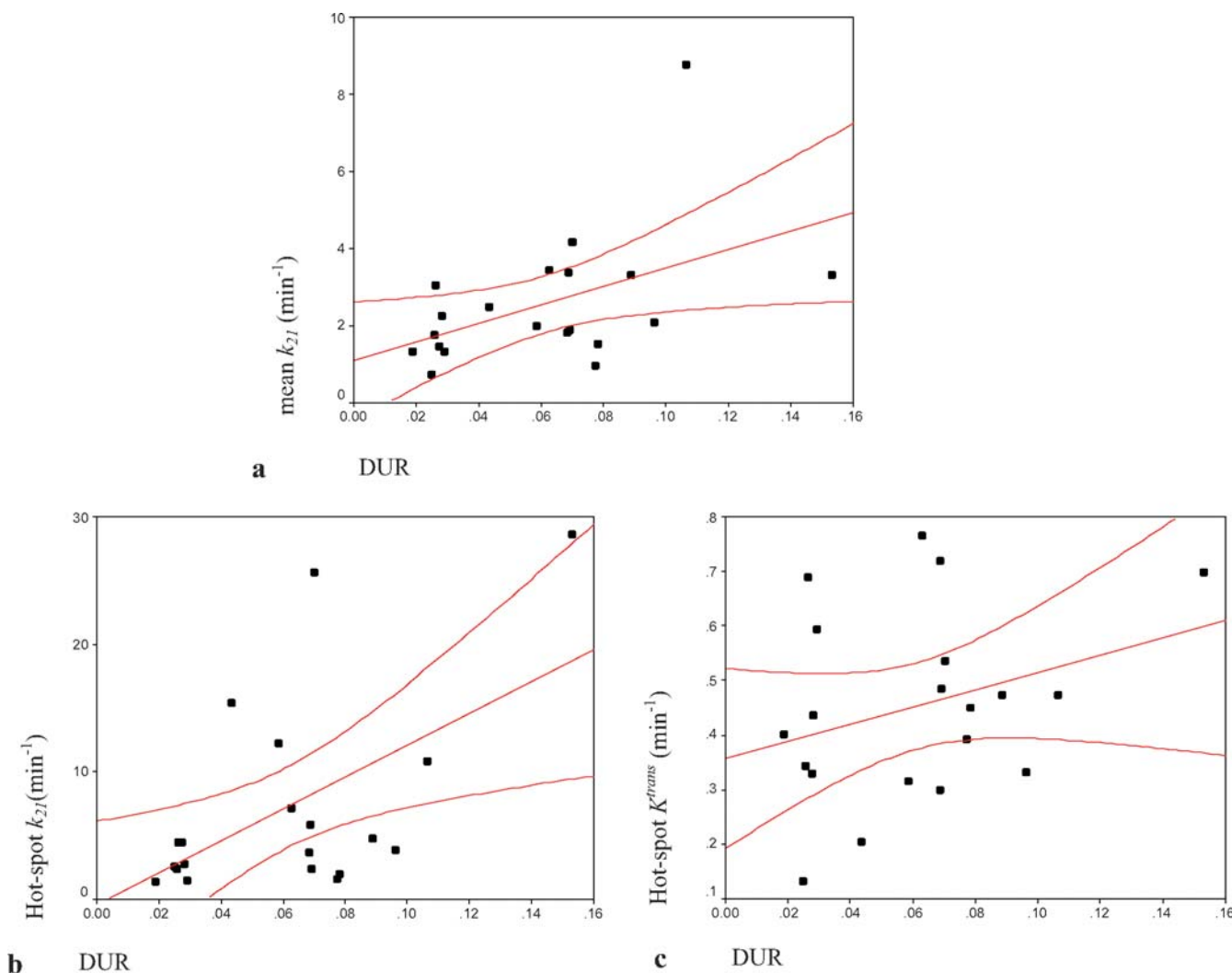


Fig. 5 a–c Significant association observed between FDG differential uptake ratio (*DUR*) and MR parameters, **a** mean tumour uptake curve Brix parameter k_{21} ($\eta^2=0.27$, $P=0.028$) ($P_S=0.5$, $P=0.026$), **b** hot-spot Brix parameter k_{21} ($\eta^2=0.44$, $P=0.003$), **c** hot-spot Tofts parameter K^{trans} ($\eta^2=0.33$, $P=0.010$). Each parameter distribution is displayed with best line fit and 95% confidence intervals. Associations tested using application of the general linear model. Spearman's correlation coefficient was also calculated for mean k_{21} values

In previous studies investigating pharmacokinetic analysis in breast cancer, workers have analysed the data using non-parametric statistics. In particular Brix et al. [15] used a Spearman correlation to test for associations between PET and MRI values. In order to compare our work with the result published in the paper by Brix et al. [15] we re-analysed our data using a Spearman's correlation test using the mean curve Brix model data. The Spearman's correlation analysis yielded a weak but significant correlation ($|P_S|=0.50$, $P=0.026$) between the Brix parameter k_{21} and *DUR*, whilst no other significant

correlation was observed between the other Brix parameters and *DUR*.

Discussion

The combined application of DCE-MRI and ¹⁸F-FDG PET in the assessment of breast cancer has been demonstrated previously for the evaluation of tumour recurrence after initial therapy [23, 24] and initial diagnosis [15]. Although MRI and ¹⁸F-FDG PET have been found to be complementary forms of analysis, no direct correlation has been found between parameters derived from the two forms of analysis [15]. Our study demonstrates a significant association between PET FDG uptake and DCE-MRI analysis using two multi-compartment models [18–20].

General linear modelling demonstrated that the mean curve k_{21} , hot-spot k_{21} and hot-spot K^{trans} values all demonstrated significant association with *DUR* values, as demonstrated by the η^2 values. The non-parametric anal-

ysis found a weak but significant correlation $P_5=0.5$. The choice of parametric or non-parametric statistics to analyse data such as this is still open to debate. Although we have tested our data and found that it does not differ from a normal distribution, our numbers were small ($n=20$). These results clearly demonstrate a relationship between the exchange rate constants of MRI contrast enhancement (associated with the vascular characteristics of the tumour) and DUR uptake (associated with the metabolic characteristics of the tumour).

The contradiction between our conclusions and those of previously published work may be due to several factors. The patient population examined in this study was larger and more homogeneous [19 patients presenting with invasive ductal carcinoma (IDC)], whereas the population examined by Brix et al. [15] exhibited a range of histopathologies. Our study benefits from modifications made to improve the “goodness of fit” of the models to the MR enhancement curves with the application of an accurate T_1 estimation for the Tofts model [17] and a multiple starting point approach to curve fitting [21]. It is unclear whether previous authors implemented this multiple starting point approach. Several factors may also affect the PET data analysis. Brix et al. [15] utilise a 3D PET FDG acquisition, whereas the PET data presented in our study was acquired in a 2D mode. Additionally, in the calculation of SUV presented in the study by Brix et al. [15], body weight was used. Since FDG does not accumulate in fatty tissue, using body weight may result in an error in SUV calculation. The calculation of DUR presented in our study was made using body surface area rather than body weight, which previously has been shown to compensate for this potential error [25]. Lastly, as the patient population in the study by Brix et al. [15] presented with a wider range in tumour volumes, a partial volume correction was applied to their PET data. However, there may still be some variability in measured uptake in tumours of different sizes. The patients in our studied population all featured tumours categorised as large or locally advanced such that no partial volume correction was therefore applied.

Although the potential for operator bias is minimised in our analysis by use of a semi-automated analysis technique, the definition of ROIs in each modality is a possible source of error. An ideal solution would be to register spatially the images from each modality and define a single ROI for both. However, in our experience, considerable deformation of breast tissue occurs between PET and MRI scans, even though the patient may be placed in a similar position. The non-rigid nature of breasts and the lack of anatomical detail in PET studies makes the evaluation of any registration technique difficult. In the future, problems such as these may be overcome with hybrid imaging systems such as PET/CT.

The Tofts model assumes a standardised elimination rate for every patient [18, 21] based on data obtained

from a group of healthy volunteers [26]. In contrast, the Brix model allows a different k_{el} for each voxel (as shown in Tables 2, 3) [19–21]. This allows for improved fitting of enhancement curves that do not display a significant wash-out phase. Therefore, one potentially useful modification to the data acquisition protocol employed in this study would be to obtain additional dynamic frames much longer after contrast injection such that detection of contrast wash-out would be guaranteed, allowing the Tofts model to fit the data more robustly.

One possible explanation of the correlation between DCE-MRI and ^{18}F -FDG PET is that FDG delivery to the tumour is limited by the flow dynamics of the tumour, a measure of which are the exchange rate constants associated with the MR models. Our results indicate that care must therefore be taken during analysis of ^{18}F -FDG PET data from large tumours. If uptake is calculated for such a tumour, the calculation used must take into account the possibility that certain regions of tumour may display a lack of FDG uptake due to delivery restrictions. These regions may still contain some latent metabolic potential [1].

A more comparable measure of metabolic activity in relation to the vascular system of the tumour might be obtained using dynamic ^{18}F -FDG uptake allowing modelling of the vascular component of ^{18}F -FDG uptake [27]. A relationship has been demonstrated in untreated primary breast cancers between metabolic uptake and blood flow using dynamic ^{18}F -FDG and ^{15}O -water PET imaging, respectively [28]. Furthermore, it has been established that high pre-therapy tumour metabolism may be associated with a poor response to neoadjuvant chemotherapy and that a low ratio of metabolism to blood flow may successfully predict improved response to chemotherapy in large or locally advanced breast cancers (LABC) [29]. It has also been demonstrated that, whilst responsive and unresponsive LABC tumours display an average decline in dynamic ^{18}F -FDG uptake as a result of chemotherapy, tumours that are resistant to therapy will display an increase in ^{15}O -water blood flow during the therapy regimen [30].

Our study establishes an association between a potential surrogate measure for drug delivery and tumour metabolism using DCE-MRI and static ^{18}F -FDG uptake. Further investigation of this relationship is therefore warranted in larger patient trials. The usefulness of such a measure may be further established by investigating its value in assessing tumour response. This is a direction for future work.

References

1. Semple SIK, Gilbert FJ, Redpath TW, Ahearn TS, Welch AE, Hutcheon AW, Heys SD, Smyth EH, Miller ID, Smith IC (2003) Correlation of MRI-PET rim enhancement in breast cancer. A delivery related phenomenon with therapy implications? *Lancet Oncol* 4:759
2. Heywang SH (1994) Contrast enhanced magnetic resonance imaging of the breast. *Invest Radiol* 29:94–104
3. Flickinger FW, Allison JD, Sherry RM, Wright JC (1993) Differentiation of benign from malignant breast masses by time-intensity evaluation of contrast-enhanced MRI. *J Magn Reson Imaging* 11:617–620
4. Tsuboi N, Inomata T, Ogawa Y, Yoshida D, Yoshida S, Moriki T, Kumon M (1999) Changes in the findings of dynamic MRI by preoperative CAF chemotherapy for patients with breast cancer of stage II and III: pathologic correlation. *Oncol Rep* 6:727–732
5. Kuhl CK (2000) MRI of breast tumors. *Eur Radiol* 10:46–58
6. Hayes C, Padhani AR, Leach MO (2002) Assessing changes in tumour vascular function using dynamic contrast-enhanced magnetic resonance imaging. *NMR Biomed* 15:154–163
7. Rieber A, Brambs H-J, Gabelmann A, Heilmann V, Keinberg R, Kühn T (2002) Breast MRI for monitoring response of primary breast cancer to neo-adjuvant chemotherapy. *Eur Radiol* 12:1711–1719
8. Tofts PS, Berkowitz B, Schnall MD (1995) Quantitative analysis of dynamic Gd-DTPA enhancement in breast tumours using a permeability model. *J Magn Reson Med* 33:564–568
9. Hoffman U, Brix G, Knopp MV, Heß T, Lorenz WJ (1995) Pharmacokinetic mapping of the breast: a new method for dynamic mammography. *J Magn Reson Med* 33:506–514
10. Bombardieri E, Crippa F, Maffioli L, Greco M (1997) Nuclear medicine techniques for the study of breast cancer. *Eur J Nucl Med* 24:809–824
11. Flanagan FL, Dehdashti F, Siegel BA (1998) PET in breast cancer. *Semin Nucl Med* 28:290–302
12. Wahl RL, Zasadny K, Helvie M, Hutchins GD, Weber B, Cody R (1993) Metabolic monitoring of breast cancer chemohormonotherapy using positron emission tomography: initial evaluation. *J Clin Oncol* 11:2101–2111
13. Bassa P, Kim EE, Inoue T, Wong FCL, Korkmaz M, Yang DJ, Wong WH, Hicks KW, Buzdar AU, Podoloff DA (1996) Evaluation of preoperative chemotherapy using PET with fluorine-18-fluorodeoxyglucose in breast cancer. *J Nucl Med* 37:931–938
14. Smith IC, Welch AE, Hutcheon AW, Miller ID, Payne S, Chilcott F, Waikar S, Whitaker T, Ah-See AK, Eremin O, Heys SD, Gilbert FJ, Sharp PF (2000) Positron emission tomography using [¹⁸F]-fluorodeoxy-D-glucose to predict the pathologic response of breast cancer to primary chemotherapy. *J Clin Oncol* 18:1676–1688
15. Brix G, Henze M, Knopp MV, Lucht R, Doll J, Junkermann H, Hawighorst H, Haberkorn U (2001) Comparison of pharmacokinetic MRI and [¹⁸F] fluorodeoxyglucose PET in the diagnosis of breast cancer: initial experience. *Eur Radiol* 11:2058–2070
16. Wienhard K, Eriksson K, Grootoink S, Casey M, Pietrzyk U, Heiss WD (1992) Performance evaluation of the positron scanner ECAT EXACT. *J Comput Assist Tomogr* 16:804–813
17. Semple SIK, Redpath TW, Ahearn TS, Gilbert FJ, Hutcheon AW, Heys SD (2003) Effect of accurate T1 calculation on pharmacokinetic analysis of primary breast cancer. In: Proceedings of the 11th annual meeting of ISMRM, Toronto, Canada
18. Tofts PS, Kermode AG (1991) Measurement of the blood-brain barrier permeability and leakage space using dynamic MR imaging. 1. Fundamental concepts. *J Magn Res Med* 17:357–367
19. Brix G, Semmler W, Port R, Schad LR, Layer G, Lorenz WJ (1991) Pharmacokinetic parameters in CNS Gd-DTPA enhanced MR imaging. *J Comput Assist Tomogr* 15:621–628
20. Knopp MV, Brix G, Junkermann HJ, Sinn HP (1994) MR mammography with pharmacokinetic mapping for monitoring of breast cancer treatment during neoadjuvant therapy. *Magn Reson Imaging Clin N Am* 2:633–658
21. Tofts PS, Brix G, Buckley DL, Eveloch JL, Henderson E, Knopp M, Larsson HBW, Lee T-Y, Mayr NA, Parker GJM, Port RE, Taylor J, Weisskoff RM (1999) Estimating kinetic parameters from dynamic contrast-enhanced T₁-weighted MRI of a diffusible tracer: standardized quantities and symbols. *J Magn Reson Imaging* 10:223–232
22. Ahearn TS (2003) The accuracy and robustness of dynamic contrast enhanced magnetic resonance imaging methodology. Ph.D Thesis, University of Aberdeen, pp 159–174
23. Hathaway PB, Mankoff DA, Maravilla KR, Austin-Seymour MM, Ellis GK, Gralow JR, Cortese AA, Hayes CE, Moe RE (1999) Value of combined FDG PET and MR imaging in the evaluation of suspected recurrent local-regional breast cancer: preliminary experience. *Radiology* 210:807–814
24. Goerres GW, Michel SCA, Fehr MK, Kaim AH, Steinert HC, Seifert B, von Schulthess GK, Kubik-Huch RA (2003) Follow-up of women with breast cancer: comparison between MRI and FDG PET. *Eur Radiol* 13:1635–1644
25. Kim CK, Gupta NC, Chanramouli B, Alavi A (1994) Standardized uptake values of FDG: body surface area correction is preferable to body weight correction. *J Nucl Med* 35:164–167
26. Weinmann HJ, Laniado M, Mutzel W (1984) Pharmacokinetics of Gd-DTPA/Dimeglumine after intravenous injection into healthy volunteers. *Physiol Chem Phys Med NMR* 16:167–172
27. Williams KV, Bertoldo A, Mattioni B, Price JC, Cobelli C, Kelley DE (2003) Glucose transport and phosphorylation in skeletal muscle in obesity: insight into a muscle-specific positron emission tomography model. *J Clin Endocrinol Metab* 88:1271–1279
28. Zasadny KR, Tatsumi M, Wahl RL (2003) FDG metabolism and uptake versus blood flow in women with untreated primary breast cancers. *Eur J Nucl Med Mol Imaging* 30:274–280
29. Mankoff DA, Dunnwald LK, Gralow JR, Ellis GK, Charlop A, Lawton TJ, Schubert EK, Tseng J, Livingston RB (2002) Blood flow and metabolism in locally advanced breast cancer: relationship to response to therapy. *J Nucl Med* 43:500–509
30. Mankoff DA, Dunnwald LK, Gralow JR, Ellis GK, Schubert EK, Tseng J, Lawton TJ, Linden HM, Livingston RB (2003) Changes in blood flow and metabolism in locally advanced breast cancer treated with neoadjuvant chemotherapy. *J Nucl Med* 44:1806–1814